Journal of Biomechanical Science and Engineering

Vol. 3, No. 2, 2008

Remodeling of Endothelial Cell Nucleus Exposed to Three Different Mechanical Stimuli *

Toshiro OHASHI**, Kazuhiko HANAMURA**, Daisaku AZUMA**, Naoya SAKAMOTO** and Masaaki SATO**

**Department of Bioengineering and Robotics, Graduate School of Engineering, Tohoku University
6-6-01 Aoba-yama, Sendai 980-8579, Japan
E-mail: ohashi@bml.mech.tohoku.ac.jp

Abstract

Cell Nuclei play a critical role in controlling gene expression and replicating DNA, and is known to deform in association with cell shape changes in response to external forces. This study dealed with morphological analysis to quantitatively assess the effect of three different mechanical stimuli including fluid shear stress, cyclic stretching, and hydrostatic pressure on nucleus morphology. Fluorescence images showed that fluid shear stress and cyclic stretching induced cell elongation and orientation very specifically to the direction of flow and stretch, respectively. In contrast, hydrostatic pressure induced cell elongation at non-preferred orientation. The nuclei were also found to deform in the same manner as that of the cells, which was, in particular, dependent on the type of mechanical stimuli, possibly suggesting the direct mechanical linkages between cell surface receptors, cytoskeletal meshworks, and nuclei. It was also shown that cytoskeletal meshworks may contribute to pre-existing strain of the nuclei.

Key words: Endothelial Cells, Nucleus Remodeling, Shear Stress, Cyclic Stretching, Hydrostatic Pressure, Cytoskeletal Meshworks

1. Introduction

A lot of efforts have been exclusively made to explore the effect of fluid shear stress on vascular endothelial cell responses including changes in morphology and cytoskeletal structures particularly with implications for the localization of atherosclerosis [1]-[4]. When endothelial cells are exposed to fluid shear stress, cells exhibit marked elongation and orientation in the direction of flow, possibly leading to alterations in several aspects of endothelial cell biology that are critical to normal endothelium functions [5]. Since endothelial cells are exposed to complex mechanical forces in vivo including not only fluid shear stress but also stretching and hydrostatic pressure, it is critical to understand how the other two mechanical stimuli can affect endothelial cell responses. Application of cyclic stretching induces endothelial cell alignment almost perpendicular to the direction of stretch [6],[7]. In contrast, endothelial cells exposed to hydrostatic pressure exhibit elongation with non-preferred orientation [8],[9]. These studies thus indicate that morphological responses in endothelial cells may depend on the types of mechanical stimuli.

Although endothelial cell responses to mechanical stimuli have been well understood so far, little is still known of how endothelial cell nuclei may change their shapes in association with mechanical stimuli-induced cell shape changes. The major function of the cell nuclei is to control gene expression and mediate the replication of DNA during the cell cycle, which can be modulated by external forces. For example, twisting integrin receptors with RGD-containing peptide-coated beads increased endothelin-1 gene expression under the

*Received 26 Nov., 2007 (No. 07-0765)
[DOI: 10.1299/jbse.3.63]

hypothesis that the molecular structural linkage of integrin-cytoskeleton is an important pathway for the mechanotransduction [10]. Furthermore, when integrins were pulled by the RGD-coated miropipettes or microbeads, cell nuclei distorted and nucleoli redistributed along the direction of the applied force [11]. It has been known that nucleus deformation can be associated with cell deformation when cells are exposed to fluid shear stress [12], compression [13], stretching [14], and flatten [15], indicating direct mechanical linkages between cell surface receptors, cytoskeletons, and nuclei. To further address endothelial cell responses to mechanical forces, cell nucleus responses should be thus explored.

The objective of this study was to precisely quantify the effect of three different mechanical stimuli including fluid shear stress, cyclic stretching, and hydrostatic pressure on endothelial cell nucleus morphology. Mechanical contributions of cytoskeletal meshworks on nucleus morphology were also assessed after treatments with disruptive reagents.

2. Materials and methods

2.1. Cell culture

Bovine aortic endothelial cells were purchased from Cell Applications (San Diego, CA, USA). Endothelial cells were seeded into a tissue culture flask (Sumilon, Tokyo, Japan) with Dulbecco's modified Eagle medium (DMEM, Invitrogen, MD, USA) supplemented with 10% heat-inactivated fetal bovine serum (JRH Biosciences, KS, USA), penicillin and streptomycin (Invitrogen) and cultured at 37°C in a 5% CO_2/ 20% O_2/ 75% N_2 environment. Cells were confluent after 4-5 days and then passaged at a 1:4 split ratio in the flask using 0.05% trypsin-EDTA (Invitrogen). Before experiments, cells were seeded on a non-coated custom-built glass base culture dish with a diameter of 35 mm (Asahi Techno Glass, Tokyo, Japan) designed to allow shear stress- or hydrostatic pressure-imposed experiments. Cells were also seeded on a 0.1% gelatin-coated rectangular silicone membrane attached to the bottom of a silicone chamber for cyclic stretching-imposed experiments (see 2.2). Fully confluent cell populations from the 4th to 10th generation were studied.

2.2. Application of three different mechanical stimuli

The effect of three different mechanical stimuli, fluid shear stress, cyclic stretching and hydrostatic pressure, on nucleus morphology were studied with experimental methods previously reported [7],[8],[16]. Schematic diagrams of the experimental setup are shown in Fig. 1.

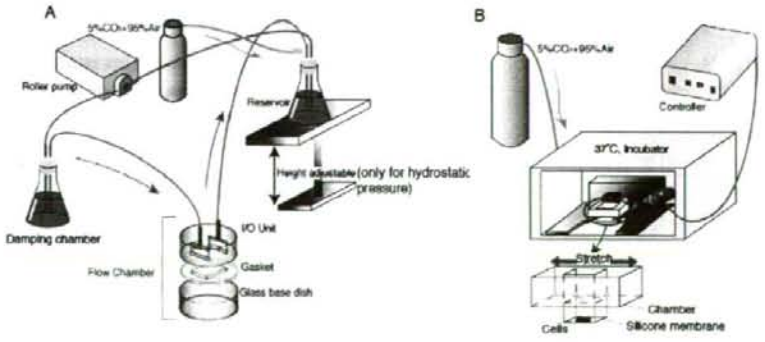

Fig. 1 Schematic diagram of experimental setup for (A) fluid shear stress-imposed and hydrostatic pressure-imposed experiments and (B) cyclic stretching-imposed experiment.

For fluid shear stress-imposed experiments, the confluent cell monolayer was loaded into a parallel-plate flow chamber, as shown in Fig. 1A. In the flow chamber, an input/output (I/O) unit and a gasket were set in the glass-base dish to compose a flow field having a flow section of 0.5 mm in height and 14 mm in width. The channel flow can be approximated as two-dimensional fully developed laminar flow. Fluid shear stress of 2 Pa, which is comparable to the average value in aorta, was applied to cells for 24 h using a flow circuit consisting the flow chamber, two reservoirs, and a roller pump (Master Flex, IL, USA). During cell loading, the temperature of culture medium was maintained at 37°C by placing the damping chamber in a thermostatic chamber, and the pH controlled by pumping mixed gas (5% CO_2/ 20% O_2/ 75% N_2).

For application of hydrostatic pressure, a similar assembly to that used for the fluid shear stress-imposed experiments was used. The height of the reservoir controls the hydrostatic pressure applied to the endothelial cell monolayer in the flow chamber. Using this system, hydrostatic pressures of 100 mmHg representing mean blood pressures in aorta was applied to the monolayer for 24 h. It should be noted that very slow fluid flow with shear stress of less than 0.1 Pa was applied to cells to perfuse nutrients and oxygen.

For cyclic stretching experiments, a silicone chamber (10 mm high x 25 mm wide x 44 mm long) with a cells-seeded silicone membrane having a square region of 20 mm x 20 mm was mounted on a commercially available cyclic stretcher consisting of a stepping motor and a controller (NS-600, Strex, Osaka, Japan), as shown in Fig. 1B. Prior to cell seeding, the silicone membrane was coated with 0.1% gelatin (Sigma, MO, USA). The silicone chamber was cyclically stretched up to a maximum strain of 10% at a frequency of 0.5 Hz for 6 h.

Each loading time were chosen to allow cells to undergo complete remodeling, referring to previous studies.

2.3. Disruption of cytoskeletal meshworks

In order to know how cytoskeletal meshworks can contribute to nucleus shape, actin filaments, intermediate filaments, and microtubules in unstimulated control cells were disrupted with treatment of 1 μg/ml cytochalasin D for 30 min at 37°C, 1 μM colchicines for 1 h at 37°C, and 5 mM acrylamide for 5 h at 37°C, respectively. Cell nuclei and cytoskeletons were fluorescently observed and morphological parameters of cell nuclei were analyzed (see 2.4 and 2.5).

2.4. Immunofluorescence staining

After mechanical tests, cells were incubated with 1 μg/ml CM-DiI (Molecular Probes, OR, USA) for 15 min at 4°C for staining cell membrane followed by an incubation with 0.4% SYTO13 (Molecular Probes), a marker of nucleic acids, for 20 min at 37°C for staining cell nuclei. Cells were also fixed with 10% formaldehyde in PBS (Dulbecco's phosphate-buffered saline without Ca^{2+} or Mg^{2+}, Wako, Osaka, Japan) for 5 min, permeabilized with 0.1% Triton X-100 in PBS for 5 min, and then incubated with 150 nM rhodamine-phalloidin (Molecular Probes) for 20 min at room temperature (RT) to study the effect of remodeling of actin meshwork on nucleus morphology.

For cytoskeleton disruption experiments, cells were incubated with 0.4% SYTO13 for 20 min at 37°C for staining cell nuclei before the disruption. After the disruption, cells were fixed with 10% formaldehyde in PBS for 5 min, permeabilized with 0.1% Triton X-100 in PBS for 5 min, and then incubated with 150 nM rhodamine-phalloidin for 20 min at RT, an anti-vimentin antibody (ProGen Biologics, MO, USA) for 20 min at RT followed by a Alexa Fluor 455-labelled anti-rabbit IgG antibody (Invitrogen) for 40 min at RT, and FITC-labelled anti-α-tubulin (Sigma) for 20 min at RT, for staining actin filaments, intermediate filaments, and microtubules, respectively. Nucleus shape and cytoskeletal

meshworks were fluorescently observed before and after the disruption.

Fluorescence images were captured using a confocal laser scanning microscope (FV1000, Olympus, Tokyo, Japan) with a 60x, NA 1.4 oil immersion objective (Uplan Apo, Olympus) as a series of X-Y optical slices at 0.35 μm on Z axis.

2.5. Morphological Analysis

Morphological parameters of the nuclei including angle of orientation, Shape index [17], projected area, and volume were evaluated using the public domain software (Image J 1.36b, National Institutes of Health, MD, USA). The cell outline was semi-automatically extracted producing cell area and perimeter. An equivalent ellipse for the cell outline, with an equal area and moment of inertia to the corresponding cell shape was then determined. The angle of orientation is defined as the deviation of the major axis of the equivalent ellipse from the direction of flow, by setting the cell orientation to a value ranging from 0° to ± 90°. For all images, the horizontal direction from left to right was defined as 0°. The angle of orientation was also evaluated for the cells. The shape index is defined as follows.

$$\text{Shape index} = 4\pi A / P^2 \qquad (1)$$

where A is the cell area, and P the cell perimeter. The shape index is defined as 1.0 for a circle and approaches zero for highly elongated shape. Three-dimensional volume measurement of the nuclei was performed from the rendered images using a series of confocal slices.

2.6 Statistical Analysis

Statistical comparisons were made using unpaired Student's t-test and unpaired Welch's t-test for equal variance and unequal variance, respectively, unless otherwise stated. A value of $p < 0.05$ was considered significant in all analyses. Statistical data were shown as mean + SD or mean ± SD.

3. Results

3.1. Effects of mechanical stimuli on nucleus morphology

Fluorescence images of nucleus and cell membrane after the application of the three different mechanical stimuli were shown in Fig. 2. Changes in nucleus morphology were clearly observed in response to the mechanical stimuli, showing a close association with cell shape change. Actin meshwork for the three separate experiments was also shown in the figure. The actin cytoskeletons responded specifically to the three different mechanical stimuli. Statically cultured control cells exhibited a rounded shape, and thin, short actin filaments were centrally observed together with dense peripheral bands of actin filaments at the cell periphery. After exposure to fluid shear stress, cells exhibited elongation and orientation in the direction of flow with centrally located thick stress fibers parallel to the direction of flow, whereas, after exposure to cyclic stretching, cells elongated and oriented nearly perpendicular to the direction of stretch with thick stress fibers aligned with the major axis of cells. In contrast, cells exposed to hydrostatic pressure exhibited elongated shape with non-preferred orientation, with peripherally located long and thick filaments.

The angles of orientation of cells and their nuclei were shown in Fig. 3 for the three mechanical stimuli. For control cells, the angle of cell orientation was uniformly distributed between angles approaching -90° or 90°. The similar tendency was observed for the angle of nucleus orientation. The percentages of sheared cells aligning between - 30° and + 30° were approximately 60% and 70% for the cells and their nuclei, respectively, indicating a close association of the cells with the nuclei in morphological change. Furthermore, the

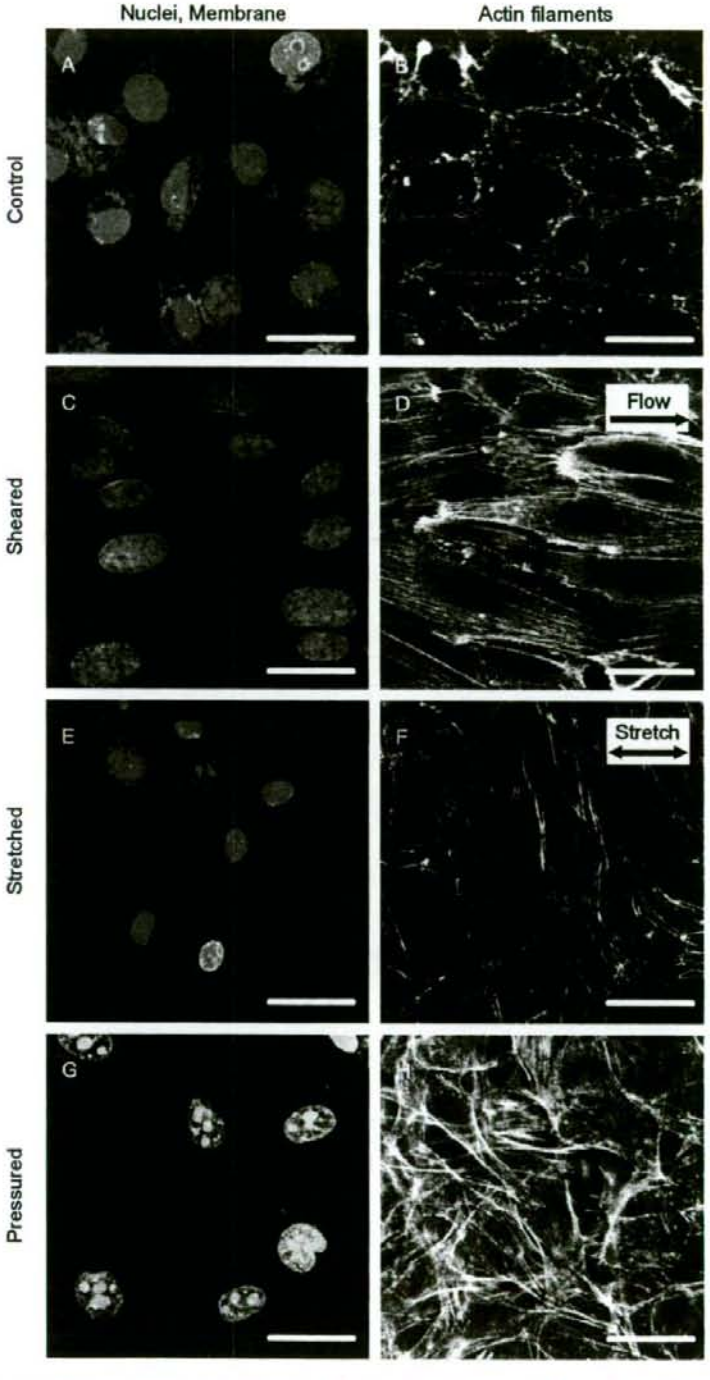

Fig. 2 Fluorescence images of (A, C, E, G) cell nuclei and membrane and (B, D, F, H) actin filaments for statically cultured control, sheared, stretched, and pressured cells. Bars = 30 μm.

percentages of stretched cells aligning between ± 60° and ± 90° were approximately 62% and 50% for the cells and their nuclei, respectively. In contrast, for pressured cells, the cells and their nuclei randomly aligned between - 90° and + 90° and no perceptive difference was found. However, there was a positive correlation between the cells and their nuclei in angle of orientation (Pearson's Product-Moment Correlation Coefficient r =0.633, $p < 0.001$).

Figure 4 shows the shape indices of the nuclei for the three mechanical stimuli. There were significant difference between both sheared (0.83 ± 0.05) and stretched cells (0.84 ±

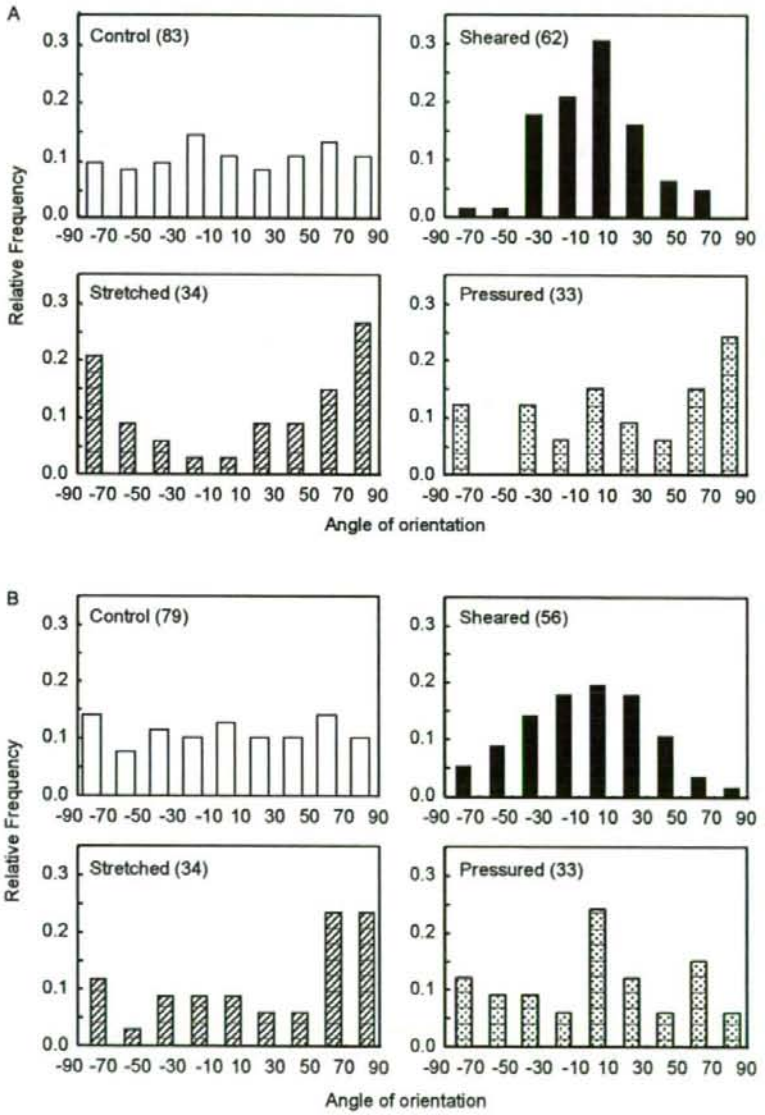

Fig. 3 Change in the angle of orientation for (A) cells and (B) their nuclei after application of the three mechanical stimuli. The number in the parenthesis indicates the number of cells.

0.07) and control cells (0.87 ± 0.04, $p < 0.01$ vs. sheared and stretched cells), whereas no significant difference between pressured cells (0.86 ± 0.06) and control cells.

The nucleus area and volume are shown in Figs. 5A and 5B, respectively for the three mechanical stimuli. In the area, compared to control cells (138 ± 63), a significant increase was found only in pressured cells (177 ± 57). No significant differences were found under the other two conditions (125 ± 34 and 139 ± 57 for sheard and stretched cells, respectively). After exposure to mechanical stimuli, compared to control cells (825 ± 295),

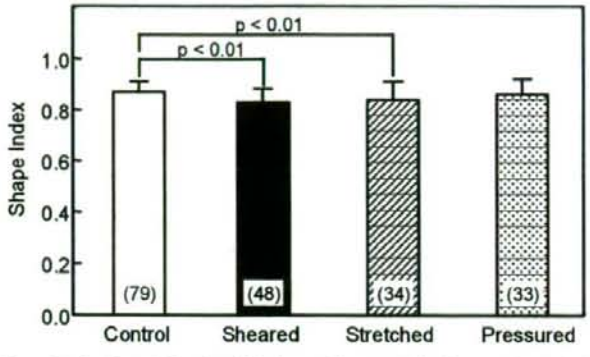

Fig. 4 Change in the shape index of nuclei after application of the three mechanical stimuli. The number in the parenthesis indicates the number of cells.

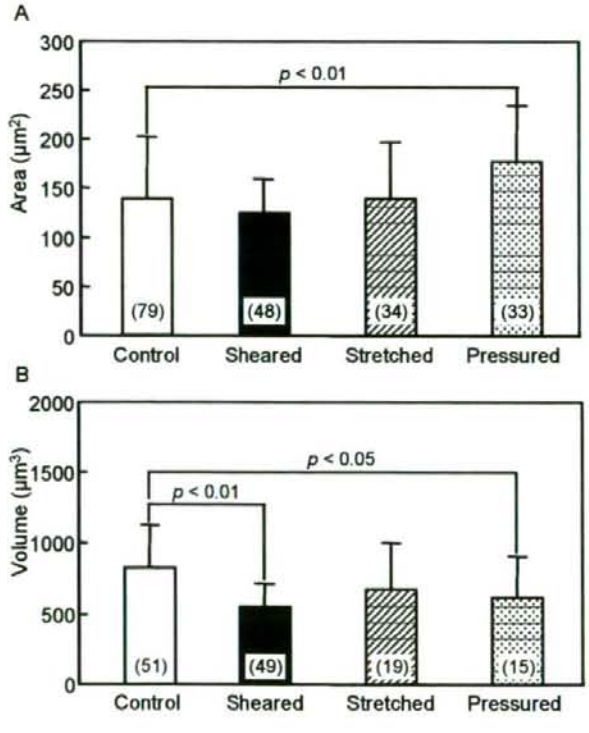

Fig. 5 Changes in (A) area and (B) volume of nuclei after application of the three mechanical stimuli. The number in the parenthesis indicates the number of cells.

the nucleus volume significantly decreased for sheared cells (553 ± 162, $p < 0.01$) and pressured cells (620 ± 284, $p < 0.05$), whereas the volume decreased on average but there was no significant for stretched cells (676 ± 322). Taken together, these results indicate that the morphological change of the nuclei is not in an isotropic manner, and not likely due to passive deformation caused by the change in the their surrounding mechanical environment such as development of stress fibers, but rather due to the active remodeling in response to mechanical stimuli, because cell nuclei can be assumed to be incompressible.

3.2. Effects of cytoskeletal disruptions on nucleus morphology

It was confirmed from fluorescence studies that actin filaments, intermediate filaments, and microtubules were well disrupted after treatment with the disruptive reagents. Changes in morphological parameters including the shape index, area, and volume of the nuclei after the disruption are shown in Fig. 6. The shape index showed no significant differences under the three conditions. Significant decreases were found in area under the three conditions ($p < 0.05$). No significant difference was found in volume for disruption of actin filaments, whereas a significant increase was found for disruption of intermediate filaments ($p < 0.05$). Disruption of microtubules induced a significant decrease in volume ($p < 0.05$).

4. Discussion

The findings of this study indicate that the nuclei change their shape in accordance with different types of mechanical stimuli including fluid shear stress, cyclic stretching, and hydrostatic pressure, in a similar manner to that of the cells. Flaherty et al. [18] reported that endothelial cell nuclei showed differences in morphology at different locations around the circulatory system in canine. In regions of stronger hemodynamic forces, such as large arteries, the nuclei were elliptical in shape with their major axes being aligned with the direction of flow, whereas, in regions of weaker hemodynamic forces, the nuclei were more rounded and had no preferential direction. Flaherty et al. [18] also surgically changed the direction of flow exposed to the nuclei and found that the nuclei reoriented themselves in order to remain aligned with the flow. In this study, in vitro experiments here demonstrated that fluid shear stress may induce nucleus elongation and orientation in the direction of flow, which is in good agreement with the previous in vivo experiment.

Unlike fluid shear stress and hydrostatic pressure, cyclic stretching is defined as a strain-controlled mechanical loading. Therefore, it is important to pay particular attention to the terms, "passive deformation" and "(active deformation-induced) remodeling". In

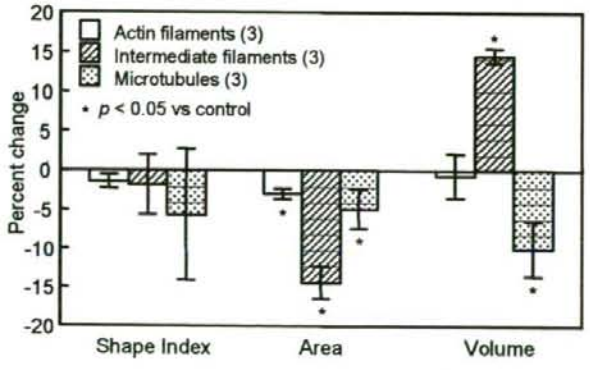

Fig. 6 Changes in the shape index, area, and volume of nuclei after disruption of the three cytoskeletons. The number in the parenthesis indicates the number of cells.

general, observing the "passive deformation" of cells and cellular components including nuclei may take seconds or minutes after application of mechanical stimuli. If the nuclei passively deform, they would experience elongation in the direction of stretch by cyclic stretching. It has been reported that the nucleus is 9 times stiffer than the rest of the cell [11]. Taken together, it seems difficult for the nuclei to exhibit passive deformation even when being stretched up to 10%. Caille et al. [14],[19] reported that cell nuclei deformed less than the cytoplasm, which can be explained by the fact that the nuclei is much stiffer than the cytoplasm. In contrast, the "remodeling" may take hours to be observed. If the nuclei do not remodel and have enough stiff to resist the externally applied mechanical forces, no change in shape would be observed. However, the nuclei clearly showed alignment perpendicular to the direction of stretch at 6 hours after exposure to cyclic stretching, similar to that of their cells. Wang et al. [6] subjected bovine endothelial cells to 10% stretching at 0.5 Hz for 3 h and found that the cells reoriented specifically towards the direction of minimal substrate deformation. Furthermore, it is interesting to note that a numerical simulation showed that endothelial cells may respond to the applied flow in such a way as to minimize the total force on their nuclei [20]. Likewise, it is possible that cell nuclei remodel so as to minimize strain energy experienced by themselves.

After application of hydrostatic pressure, the nuclei neither showed, for the first time, any preferential alignment nor elongation. In our previous study, it was reported that bovine endothelial cells showed elongation with random cell orientation under pressured conditions, resulted in a significant decrease in the shape index [8]. This is probably because hydrostatic pressure is not a unidirectional stimulation unlike fluid shear stress and cyclic stretching. Little is still known of how mechanical forces are transmitted to local mechanosensing sites including focal adhesions [21] and intercellular junctions [22] where mechanical forces would be converted into biochemical signals, and to the nucleus [11] where mechanical forces would be possibly transduced into specific genetically regulated responses. In particular, it has been shown that external forces are transmitted by direct mechanical connections between surface receptors including integrins, cytoskeletal filaments and nucleoplasm [11]. Furthermore, finite element analysis was performed to explore the mechanotransduction pathway mediated by adhesion sites, cytoskeletons, and nuclei [23]. These studies may imply that alignment of cytoskeletal meshworks should be prerequisite for the remodeling of the nuclei. Pressured cells showed peripherally developed thick actin bundles. Therefore, it is hypothesized that pressured cells may have less unidirectional mechanical coupling between the nucleus and the cell surface where external forces are applied, towards the specific directions.

For hydrostatic pressure-imposed experiments, shear stress of less than 0.1 Pa was applied to cells to perfuse nutrients and oxygen. In our previous study [8], it has been confirmed that there is no significant difference in cell morphology between cells exposed to shear stress of less than 0.1 Pa and control cells cultured statically in an incubator. Dewey et al. [24] reported that shear stress of less than 0.5 Pa did not induce any morphological change of bovine aortic endothelial cells. In contrast, Warabi et al. [25] reported that human umbilical vein endothelial cells cultured on a collagen-coated filter formed the line after exposure to low shear stress of 0.02 Pa in association with changes in gene expression. The difference in the critical shear stress may be due to the difference in the experimental conditions such as types of cells and extracellular matrices.

How cell nuclei remodel in response to mechanical stimuli is unclear. One possible idea to explain the mechanism of the nucleus remodeling would include the fact that there exists the nuclear lamina which is a fibrillar meshwork composed of intermediate filaments that lines the inner surface of the nuclear envelope. Galbraith et al. [26] applied fluid shear stress of ca. 1.5 Pa for 24 and showed that intermediate filaments aligned with the direction of fluid flow. Therefore, it is likewise possible for the cell nuclei to actively change their shape

possibly due to the reorganization of the nuclear lamina in response to mechanical stimuli.

It was also found in this study that three cytoskeletal meshworks including actin filaments, intermediate filaments, and microtubules could affect morphology of the nuclei even in statically cultured cells, indicating nucleus elastic recovery probably due to the release of mechanical constraints induced by cytoskeletal structures being the possible determinants in the deformation. However, the induced-deformation demonstrated different characteristics depending on the three types of the loss for cytoskeletons. It has been suggested that endothelial nuclei possibly have a mechanical contribution to intracellular force balances as a compression-bearing organelle, by demonstrating that the height of nuclei in cells is 0.59 of that of isolated nuclei under statically cultured conditions [12]. This implies that there exists pre-existing strain inside of the nuclei probably due to vertical compression caused by cytoskeletal meshworks. In this study, actin filaments had less contribution to the change in nucleus morphology compared to those by the other two cytoskeletons. This can be explained by the fact that well-developed actin meshwork is less distributed in the central portion of the cell, rather more at the cell periphery called dense peripheral bands. Manitois et al. [11] indicated that actin filaments potentially mediated force transfer to the nucleus at low strain and intermediate filaments effectively mediated force transfer to the nucleus. These filaments, therefore, work as molecular tensile elements as proposed separately [27]. In contrast, they also indicated that microtubules acted to hold intermediate filament lattice open and to stabilize the nucleus against lateral compression. In this study, intermediate filaments and microtubules were found to include a different mechanical role, indicating that intermediate filaments compressed the nucleus and microtubules did not. One may wonder whether microtubules can produce strong enough forces to stretch the nucleus. One possible idea to explain this include that disruption of mictotubules means the loss of a compressive element from the viewpoint of intracellular force balance, leading to further compression induced by both actin filaments and intermediate filaments, and/or disruption of microtubules not only means the loss but also may affect intermediate meshwork by means of mechanical connections suggested in the previous study [11]. This is thus still unclear, but further studies should include an observation of subsequent events induced in intermediate filaments after disruption of microtubules.

In summary, this study addressed how three different mechanical stimuli including fluid shear stress, cyclic stretching, and hydrostatic pressure affect nucleus morphology. Fluorescence images showed that fluid shear stress and cyclic stretching induced cell elongation and orientation very specifically to the directions of flow and stretch, respectively, whereas hydrostatic pressure induced cell elongation at non-preferred orientation. Quantitative analysis on morphological parameters showed that cell nuclei also deformed in a similar fashion to the remodeling of cells, possibly indicating the direct mechanical linkages between cell surface receptors, cytoskeletal meshworks, and nuclei. Mechanical contributions of cytoskeletons to nucleus morphology were also assessed, showing the importance of the fact that cytoskeletal meshworks may contribute to pre-existing strain of the nuclei. It can be concluded that cell nuclei can sense external forces and remodel themselves as if they were structurally optimized.

Acknowledgements

This study was supported by the Global Nano-Biomedical Engineering Education and Research Network Centre (Tohoku University Global COE Program) and Grant-in-aid for Scientific Research from the Ministry of Education, Culture, Sports, Science and Technology of Japan (No. 17200030).

References

(1) Levesque, M.J. and Nerem, R.M., The Elongation and Orientation of Cultured Endothelial Cells in Response to Shear Stress, *Trans ASME Journal of Biomechanical Engineering*, Vol. 107 (1985), pp. 341-347.

(2) Nerem, R.M. Levesque, M.J., Cornhill, J.F., Vascular Endothelial Morphology As an Indicator of the Pattern of Blood Flow, *Trans ASME Journal of Biomechanical Engineering*, Vol. 103 (1981), pp. 172-176.

(3) Kataoka, N. Ujita, S., Sato, M., Effect of Flow Direction on the Morphological Responses of Cultured Bovine Aortic Endothelial Cells, *Medical & Biological Engineering & Computing*, Vol. 36 (1998), pp. 122-128.

(4) Ohashi, T., Sugawara, H., Matsumoto, T., Sato, M., Surface Topography Measurement and Intracellular Stress Analysis of Cultured Endothelial Cells Exposed to Fluid Shear Stress, *JSME International Journal Series C*, Vol. 43 (2000), pp. 780-786.

(5) Davies, P.F., Flow-Mediated Endothelial Mechanotransduction. *Physiological Review*, Vol. 75, (1995), pp. 519-560.

(6) Wang, J.H.-C., Goldschmidt-Clermont, P., Wille, J., Yin, F.C.-P., Specificity of Endothelial Cell Orientation in Response to Cyclic Mechanical Stretching, *Journal of Biomechanics*, Vol. 34 (2001), pp. 1563-1572.

(7) Ohashi, T., Masuda, M., Matsumoto, T., Sato, M., Nonuniform Strain of Substrate Induces Local Development of Stress Fibers in Endothelial Cells Under Uniaxial Cyclic Stretching, *Clinical Hemorheology and Microcirculation*, Vol. 37 (2007a), pp. 37-46.

(8) Ohashi, T., Sugaya, Y., Sakamoto, N., Sato, M., Hydrostatic Pressure Influences Morphology and Expression of VE-Cadherin of Vascular Endothelial Cells, *Journal of Biomechanics*, Vol. 40, No. 11 (2007b), pp. 2399-2405.

(9) Sugaya, Y., Sakamoto, N., Ohashi, T., Sato, M., Elongation and Random Orientation of Bovine Endothelial Cells in Response to Hydrostatic Pressure: Comparison with Responses to Shear Stress, *JSME International Journal Series C*, Vol. 46, No. 4 (2003), pp. 1248-1255.

(10) Chen, J., Fabry, B., Schiffrin, E.L., Wang, N., Twisting Integrin Receptors Increases Endothelin-1 Gene Expression in Endothelial Cells, *American Journal of Physiology Cell Physiology, Vol.* 280 (2001), C1475-C1484.

(11) Maniotis, A.J., Chen, C.S., Ingber, D.E., Demonstration of Mechanical Connections Between Integrins, Cytoskeletal Filaments, and Nucleoplasm That Stabilize Nuclear Structure, *Proceedings of the National Academy of Sciences of the United States of America*, Vol. 94 (1997), pp. 849-854.

(12) Deguchi, S., Maeda, K., Ohashi, T., Sato, M., Flow-Induced Hardening of Endothelial Nucleus As an Intracellular Stress-Bearing Organelle, *Journal of Biomechanics*, Vol. 38 (2005), pp. 1751-1759.

(13) Guilak, F., Compression-Induced Changes in the Shape and Volume of the Chondrocyte nucleus, *Journal of Biomechanics*, Vol. 28 (1995), pp. 1529-1541.

(14) Caille, N., Tardy, Y., Meister, J.-J., Assessment of Strain Field in Endothelial Cells Subjected to Uniaxial Deformation of Their Substrate, *Annals of Biomedical Engineering*, Vol. 26 (1998), pp. 409-416.

(15) Ingber, D.E., Fibronectin Controls Capillary Endothelial Cell Growth by Modulating Cell Shape, *Proceedings of the National Academy of Sciences of the United States of America*, Vol. 87 (1990), pp. 3579-3583.

(16) Ohashi, T. Ishii, Y., Ishikawa, Y., Matsumoto, T., Sato, M., Experimental and Numerical Analyses of Local Mechanical Properties Measured by Atomic Force Microscopy for Sheared Endothelial Cells, *Bio-Medical Materials and Engineering*, Vol. 12, No. 3 (2002), pp. 319-327.

(17) Cornhill, J.F., Levesque, M.J., Herderick, E.E., Nerem, R.M., Kilman, J.W., Vasco, J.S., Quantitative Study of the Rabit Aortic Endothelium Using Vascular Casts, *Atherosclerosis*, Vol. 35 (1980), pp. 321-337.

(18) Flaherty, J.T., Pierce, J.E., Ferrans, V.J., Patel, D.J., Tucker, W.K., Fry, D.L., Endothelial Nuclear Patterns in the Canine Arterial Tree with Particular Reference to Hemodynamic Events, *Circulation Research*, Vol. 30 (1972), pp. 23-33.

(19) Caille, N., Thoumine, O., Tardy, Y., Meister, J.-J., Contribution of the Nucleus to the Mechanical Properties of Endothelial Cells, *Journal of Biomechanics*, Vol. 35 (2002), pp. 177-187.

(20) Hazel, A.L. and Pedley, T.J., Vascular Endothelial Cells Minimize the Total Force on Their Nuclei, *Biophysical Journal*, Vol. 78 (2000), pp. 47-54.

(21) Wang, H.-B., Dembo, M., Hanks, S.K., Wang, Y.l., Focal Adhesion Kinase Is Involved in Mechanosensing During Fibroblast Migration, *Proceedings of the National Academy of Sciences of the United States of America*, Vol. 98, No. 20 (2001), pp. 11295-11300.

(22) Davies, P.F., Zilberberg, J., Helmke, B.P., Spatial Microstimuli in Endothelial Mechanosignaling, *Circulation Research*, Vol. 92 (2003), pp. 359-370.

(23) Jean, R.P., Chen, C.S., Spector, A.A., Finite-Element Analysis of the Adhesion-Cytoskeleton-Nucleus Mechanotransduction Pathway During Endothelial Cell Rounding: Axisymmetric Model, *Trans ASME Journal of Biomechanical Engineering*, Vol. 127 (2005), pp. 594-600.

(24) Dewey, C.F., Jr., Bussolari, S.R., Gimbrone, M.A. Jr., Davies, P.F., The Dynamic Response of Vascular Endothelial Cells to Fluid Shear Stress, *Trans ASME Journal of Biomechanical Engineering*, Vol. 103, (1981), pp. 177-184.

(25) Warabi, E., Wada, Y., Kajiwara, H., Kobayashi, M., Koshiba, N., Hisada, T., Shibata, M., Ando, J., Tsuchiya, M., Kodama, T., Noguchi, N.,, Effect on Endothelial Cell Gene Expression of Shear Stress, Oxygen Concentration, and Low-Density Lipoprotein as Studied by A Novel Flow Cell Culture System, *Free Radical Biology & Medicine*,, Vol. 37, (2004), pp. 682-694.

(26) Galbraith, C.G., Skalak, R., Chien, S., Shear Stress Induces Spatial Reorganization of the Endothelial Cell Cytoskeleton, *Cell Motility and the Cytoskeleton*, Vol. 40 (1998), pp. 317-330.

(27) Ingber, D.E., Tensegrity: the Architectural Basis of Cellular Mechanotransduction, *Annual Review of Physiology*, Vol. 59, (1997), pp. 575-599.

Biomed Microdevices
DOI 10.1007/s10544-008-9247-7

Localized electrical stimulation to C2C12 myotubes cultured on a porous membrane-based substrate

Takeshi Ishibashi · Yu Hoshino · Hirokazu Kaji · Makoto Kanzaki · Masaaki Sato · Matsuhiko Nishizawa

Abstract We report a porous membrane-based cell culture device that can conduct localized electrical stimulation of a cell monolayer. The device's cell culture substrate is a microporous alumina membrane with an underlying thin poly(dimethylsiloxane) (PDMS) film spotted with holes. When electric current is generated between the device's Pt ring electrodes—one of which is placed above the cells and the other below the PDMS layer—the current density condenses at the holes in the PDMS film, and cells located above the holes can be electrically stimulated. C2C12 cells were confluently cultured on the substrate and were differentiated to myotubes. To control the stimulated area in the substrate, we attempted to seal and reopen the holes of the PDMS film by using an air bubble. Since the current pulse could be effectively blocked at the sealed holes, fluorescent Ca^{2+} transients, indicative of cellular excitation, were observed from the myotubes located above holes in the open state.

Keywords Electrical stimulation · C2C12 myotube · Ca^{2+} transient · Porous alumina membrane · Bubble-sealing

Electronic supplementary material The online version of this article (doi:**10.1007/s10544-008-9247-7**) contains supplementary material, which is available to authorized users.

T. Ishibashi · Y. Hoshino · H. Kaji · M. Sato · M. Nishizawa (✉)
Department of Bioengineering and Robotics,
Graduate School of Engineering, Tohoku University,
6-6-01 Aramaki, Aoba-ku,
Sendai 980-8579, Japan
e-mail: nishizawa@biomems.mech.tohoku.ac.jp

M. Kanzaki
Department of Biomedical Engineering,
Graduate School of Biomedical Engineering,
Tohoku University,
Biomedical BLD. 2-1 Seiryo-machi, Aoba-ku,
Sendai 980-8575, Japan

M. Sato
Department of Biomedical Engineering,
Graduate School of Biomedical Engineering, Tohoku University,
6-6-01 Aramaki, Aoba-ku,
Sendai 980-8579, Japan

H. Kaji · M. Kanzaki · M. Nishizawa
JST, CREST,
Sanbancho, Chiyoda-ku,
Tokyo 102-0075, Japan

1 Introduction

In vitro cell-based assays, an intermediate between gene- or protein-based studies and whole animal experiments, are considered a promising approach for fundamental cell biology research and drug discovery (Mohr et al. 2006; Walles et al. 2007). The use of cells that mimic specific *in vivo* behavior is believed to decrease costs while leading to more accurate prediction in the drug discovery process of screening chemical libraries. Skeletal muscle is one of the major insulin-target tissues responsible for the maintenance of whole body glucose homeostasis (DeFronzo et al. 1981; Nuutila et al. 1994), and defects in glucose uptake in skeletal muscle contribute to the insulin-resistance characteristics of type 2 diabetes (Davidson et al. 1994; Hager et al. 1991; Koistinen and Zierath 2002). Analyses of the mechanistic details of insulin- and exercise-induced glucose uptake by skeletal muscle are often performed using whole animal experiments (Hayashi et al. 1998; Karnieli et al. 1987; Klip et al. 1990; Kurth-Kraczek et al. 1999; Mu et al. 2001; Nesher et al. 1985; Wallberg-Henriksson et al. 1987; Wright et al. 2004), mainly because of the lack of available

cell culture models that clearly and accurately reflect muscle glucose disposal *in vivo*.

C2C12 myoblasts, a mouse skeletal muscle cell line, are one of the candidate cell types that can provide a skeletal muscle cell culture (Blau et al. 1983; Yaffe and Saxel 1977). C2C12 cells are well-known to differentiate into myotubes by reducing the serum concentration of the media (De Deyne 2000; Engler et al. 2004; Fujita et al. 2007; Kislinger et al. 2005; Molnar et al. 2007; Moran et al. 2002; Nedachi and Kanzaki 2006; Cooper et al. 2004; Tortorella and Pilch 2002; Tourovskaia et al. 2006). A recent report showed that Ca^{2+} transients in C2C12 myotubes can be induced by electrical pulse stimulation to accelerate assembly of functional sarcomeres and stimulate contractile activity of the cells (Fujita et al. 2007). The fact that myotubes can contract in response to electrical stimulation implies that the culture can express a glucose metabolic capacity equal to that of muscle exercise *in vivo*. However, despite the strong demand for such culture system, an efficient way to reproducibly prepare contractile C2C12 myotubes has not been well established. Typically, in the electrical stimulation of cultured muscle cells on a dish, a pair of stimulating electrodes is placed at either side of the chamber (Fujita et al. 2007; Vandenburgh et al. 2008; Johnson et al. 1994; Sathaye et al. 2006; Wilson et al. 2007). In such a configuration, most of the current induced by the electrodes polarization passes through the medium parallel to the cell surface, which cannot cause cell depolarization.

Recently, we designed and validated the function of a microsystem that can conduct electroporation-based molecule delivery to predetermined section of a cell monolayer (Ishibashi et al. 2007). The system has a permeable filter membrane that is masked on its underside by an elastic thin film stenciled with holes (Takoh et al. 2004, 2005). Also, a pair of planner electrodes is placed at either side of the cell-adherent membrane. Since a transient electric field generated between the electrodes condenses at the holes, electroporation occurs only for cells located above the holes, resulting in the localized delivery of molecules to the cell monolayer. For the work reported herein, we convert this porous membrane-based device to one that can effectively apply electrical stimulation to a monolayer of myotubes differentiated from C2C12 cells. The electric current induced by the electrodes geometrically condenses at the holes of the thin film and perpendicularly passes through the cells, resulting in their effective depolarization. In order to optically observe cellular response to the stimulation *in situ*, a pair of ring-type electrodes is placed at either side of the membrane in place of planner electrodes. Also, to select a stimulation site in the myotube monolayer, we sealed the holes of the thin film in other areas, by using bubbles.

2 Experimental

2.1 The design and construction of the localized electrical stimulation device

Figure 1 shows a schematic illustration of the device for localized electrical stimulation. The device's cell culture substrate system is a commercially available, alumina membrane culture insert (pore size=0.02 μm, NUNC cat. #161395, Thermo Fisher Scientific Inc., U.S.) which is modified by attaching a thin polydimethylsiloxane (PDMS) film on the underside. The PDMS template is a 0.1 mm thick columnar photoresist pattern on a glass plate (Takoh et al. 2004, 2005). The PDMS polymer was prepared by first pouring the prepolymer (10: 1 SILPOT 184: CATALYST SILPOT 184; both of which were purchased from Dow Corning Toray, Co. Ltd., Japan) over the glass template. Then, a smooth glass plate was placed on top of the prepolymer, and the two plates were clamped together. Finally, the plates were heated to 100°C for 1 h to cure the polymer. The polymerized PDMS film was peeled from the template and placed underneath the culture insert using the adhesive nature of PDMS to provide a tight seal (Takoh et al. 2004).

The Pt ring electrode was fabricated on a glass plate by lift-off of a sputter-deposited Pt/Ti film. The outer and inner diameters of Pt ring are 26 and 16 mm, respectively. One electrode is placed above and another below the membrane. The gap between the two electrodes is always 3 mm.

A nose of polyethylene tube (inside and outside diameters, 0.76 and 1.22 mm, respectively) is manually placed near the hole of the PDMS film under the microscope observation. The other end of the tube is connected to a syringe. The hole was sealed by an air bubble manually dispensed from the nose of the tube. Also, the sealed hole was reopened by aspirating the bubble with the syringe.

2.2 Cell culture

Murine C2C12 cells (less than six passages; American Type Culture Collection, U.S.) (Blau et al. 1983; Yaffe and Saxel 1977) were maintained in a 37°C, 5% CO_2 incubator and

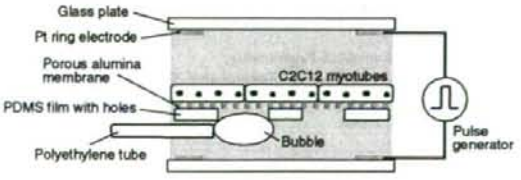

Fig. 1 Schematic illustration (cross-section) of porous membrane-based electrical stimulation device

cultured in growth media: Dulbecco's modified Eagle's medium (DMEM, Wako Pure Chemicals Industries, Ltd., Japan) containing 10% fetal bovine serum (FBS, BioWest, U.S.), 100 units mL^{-1} penicillin and 100 $\mu g\ mL^{-1}$ streptomycin (Invitrogen Corp., U.S.). When cell densities reached ~70% confluency, cells were detached by a 0.25% trypsin/0.01% EDTA solution (Invitrogen Corp., U.S.) and were either further propagated or used for experimentation.

The membrane-based substrate must be pretreated before cell culture. To prevent bubble formation in a PDMS hole during the substrate pretreatment, the substrate is first treated with O_2 plasma (60 W, 30 s) to make the polymer surface hydrophilic. Next, the substrate was immersed in a matrigel solution (3 mg mL^{-1}) (Becton, Dickson and Company, U.S.) and incubated at room temperature for 30 min. After the substrate was rinsed one time with DMEM, C2C12 cells were seeded onto the substrate at a density of 3×10^5 cells mL^{-1} and cultured until confluent. Once the cells achieved confluence, the differentiation to myotubes was induced by switching from growth medium to differentiation medium: DMEM containing 2% calf serum (Biowest, U.S.), 1 nM insulin (Sigma-Aldrich, U.S.), 100 units mL^{-1} penicillin and 100 $\mu g\ mL^{-1}$ streptomycin. The differentiation medium was changed daily (Nedachi and Kanzaki 2006). After 6 days, electrical stimulation studies were conducted.

2.3 Electrical stimulation

After assembling the device (Fig. 1), the chamber was filled with DMEM containing 2% calf serum (Biowest, U.S.), 2% MEM amino acids solution (Invitrogen Corp., U.S.), 1% MEM non-essential amino acid solution (Invitrogen Corp., U.S.), 100 units mL^{-1} penicillin and 100 $\mu g\ mL^{-1}$ streptomycin. Current pulses were induced between the two Pt ring electrodes (one placed above and the other below the cell-cultured substrate) using an electronic stimulator (SEN-7203, Nihon Kohden, Japan) coupled with an isolator unit (SS-202J, Nihon Kohden, Japan) or a DC source (2400, Keithley Instruments Inc., U.S.).

2.4 Calcium imaging

Intracellular Ca^{2+} imaging was performed during electrical stimulation using a confocal fluorescence microscope. The cultured myotubes were loaded with 10 μM Fluo-4-AM (Dojindo Laboratories, Japan) for 60 min at 37°C and washed with fresh DMEM. Cells were imaged using a confocal scanner unit (CSU21, Yokogawa Electric Corp., Japan) with a digital CCD camera (Luca, Andor Technology, U.S.) connected to a computer. Images were recorded on a computer and analyzed using a MetaMorph software (ver. 7.1.7.0, Molecular Devices, U.S.).

2.5 Simulation of the current density in a membrane-based model device

The current density distribution within the device was simulated using the finite element method and FEMLAB software (COMSOL 3.1, COMSOL AB, Sweden). The 3D model geometry mimicked that of the experimental device including the distance between the electrodes and the PDMS film hole size. However, the structure of the porous membrane was not included, which simplifies the model calculations.

3 Results and discussion

Figure 2(a) shows the simulated current density distribution for a model device that has a PDMS film with four square holes (1 $mm^2\times2$, 4 $mm^2\times2$) when the voltage between the two ring electrodes is set to 4 V_{pp}. The electric current geometrically condenses at the holes. On the other hand, when there is no film between the electrodes (Fig. 2(b)), the ring shape of the electrode is reflected in the current density distribution. The simulation results suggest that the current density will be focused on cells above the PDMS holes. Although the magnitude of the simulated current density is greater at the edge of the hole than at the center (Fig. 2(a)), cellular excitation was observed evenly in the actual

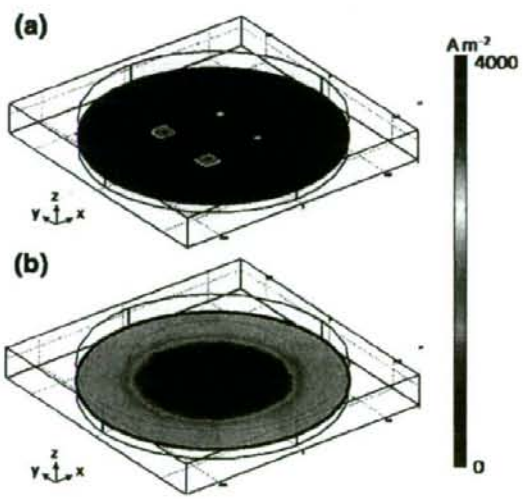

Fig. 2 Simulated current density distribution obtained for a model device (**a**) with a PDMS film with four square holes (1 $mm^2\times2$, 4 $mm^2\times2$) and (**b**) without the film, when 4 V_{pp} was set between the two ring electrodes. The length of each axis label is 2 mm

experiment, because of the morphological and electrical properties of myotubes (see below).

In order to select a localized area of the cell monolayer cultured on the membrane for stimulation, we attempted to block the electric current by using an air bubble. Figure 3 shows sequential images of the process for bubble-sealing and reopening of the PDMS hole. During sealing (images 1–5), air was ejected from the tube nose to form a bubble over the hole. As seen in image 5, the formed bubble seems to attach to the hole, due to the hydrophobic interactions between the edge of the hole and the bubble. Conversely, the sealed hole was reopened by aspirating the bubble (images 6–10). Figure 4 shows the relative AC

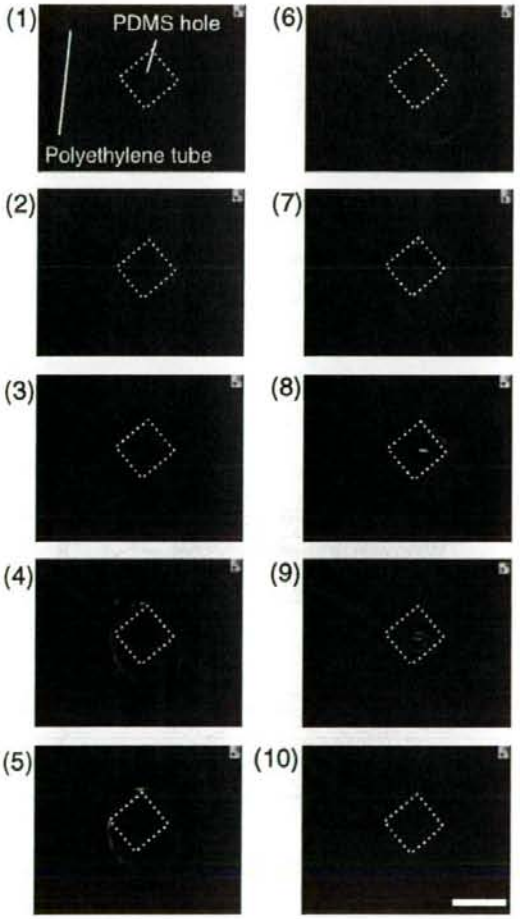

Fig. 3 Sequential (every 1 s) photographs showing the process for bubble-sealing (*1–5*) and re-opening of the PDMS hole (*6–10*). Scale bar is 1 mm

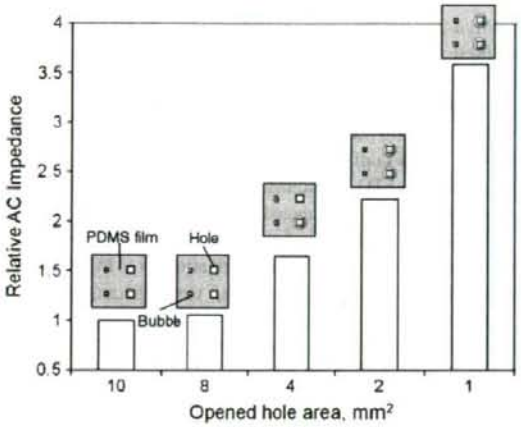

Fig. 4 Relative impedance across the porous membrane-based culture substrate, measured by using the Pt ring electrodes placed at either side of the membrane at a frequency of 10 kHz. Impedance was normalized to the value when all holes of the PDMS film were opened

impedance across the porous membrane-based culture substrate, measured with the Pt ring electrodes at a frequency of 10 kHz. The magnitude of the impedance increased as the total hole area was reduced by sealing holes with bubbles, reflecting the increase in the total resistance of the system. However, the magnitude of the impedance was not inversely proportional to the area of the opened holes, probably because the bubble-sealing did not completely block the current. Nevertheless, it is expected that the target stimulation site of the substrate can be selected because most of the current would pass through the open holes.

Figure 5(a) shows a micrograph of C2C12 myotubes cultured on the porous membrane-based substrate. The square shadow reflects a hole in the PDMS film attached underneath the membrane. As can be seen in the micrograph, elongated myotubes confluently span the hole. In order to visualize Ca^{2+} responses in myotubes during electrical stimulation, these cells were loaded with fluo-4 AM. Fluorescence images of the myotubes from open and bubble-sealed holes are shown in Fig. 5(b) and (c), respectively. Monophasic current pulses (amplitude: 4 mA, duration: 20 ms, frequency: 0.5 Hz) were generated between the two ring electrodes when one 1 mm^2 hole was opened (the others were sealed). Figure 5(d) shows the time course of relative fluorescence intensity corresponding to the changes in the cytosolic Ca^{2+} concentration at the numbered locations in Fig. 5(b) and (c). When the current pulses were applied, externally induced Ca^{2+} transients were simultaneously observed at measured points in and near the opened hole (points 1–3, Supplementary Movie 1). On the other hand, myotubes far from the opened hole (point 4) and in a

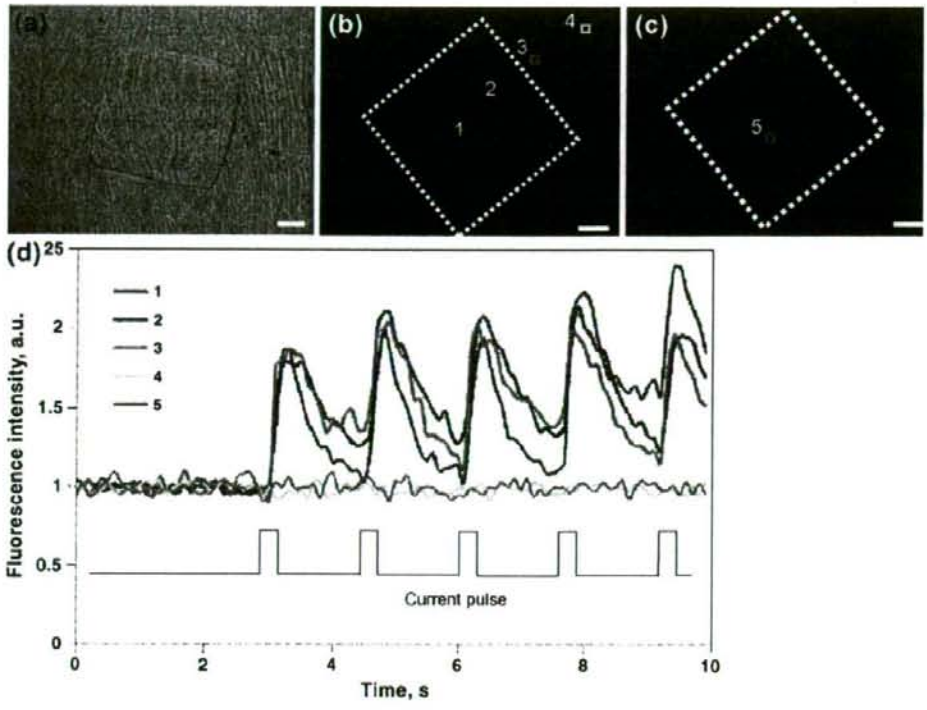

Fig. 5 (**a**) Optical image of C2C12 myotubes on the porous membrane-based culture substrate and (**b**, **c**) fluorescence images of flou-4-loaded myotubes above (**b**) the opened hole and (**c**) bubble-sealed hole. *White dotted lines* trace the boundary of the holes. Scale bar is 200 μm. (**d**) Time course of fluorescence of cytosolic Ca^{2+} measured at the points denoted in image (**b**) and (**c**) as *1–5*. Monophasic current pulse (amplitude: 4 mA, duration: 20 ms, frequency: 0.5 Hz) were applied

bubble-sealed hole (point 5) did not respond to external stimulation. The results indicate that the electric current can condense and pass through the opened hole as predicted by simulation, and bubble sealing can successfully block the current necessary for depolarization of myotubes.

A myotube forms an elongated multinuclear structure in which the fused multiple myoblasts are electrically conjugated (Lorenzon et al. 2002). Therefore, if a part of the myotube is stimulated by a current pulse, Ca^{2+} transient can occur in the whole myotube according the Ca^{2+}-induced Ca^{2+} release (CICR) mechanism (Galione and Churchill 2002). In fact, Ca^{2+} transients could be detected near the opened hole (point 3, Fig. 5), because any part of the myotube located in the hole would be stimulated. By the same logic, the Ca^{2+} transients could occur even at the center of the hole (point 1, Fig. 5) where current density is relatively lower than at the edge (see Fig. 2(a)).

Figure 6 shows the relative intensity of Ca^{2+} transients detected in the entire area of the opened hole when the amplitude of the applied current was varied while the other experimental conditions were the same as in Fig. 5. Since

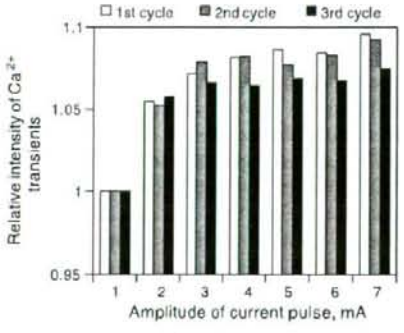

Fig. 6 Relative intensity of Ca^{2+} transients detected from the entire area of the opened hole when the amplitude of the applied current was changed from 1 to 7 mA. The fluorescence intensities of the first five transients at each given current were averaged and were then normalized to the value at the current amplitude of 1 mA. A cycle means a repeat measurement

the intensity of Ca^{2+} transients observed from an excited myotube did not greatly change across the range of applied currents (1 to 7 mA) (Supplementary Figure 1), the relative fluorescence intensity in the entire hole area corresponds to the number of myotubes that respond at the given current. As can be seen in Fig. 6, the number of responding myotubes increased as the applied current value became higher (1 to 3 mA), and it roughly reached a plateau at a value higher than 4 mA. This tendency was likewise observed in the second and third cycles of varying the applied current. The results indicate that, when using our device with a 1 mm^2 hole opened, the applied current of about 4 mA would be enough to electrically stimulate all the myotubes located above the hole. The voltage required for generating current of 4 mA between the ring electrodes was approximately 4 V, which is smaller by ten or more times than that required by conventional methods (Fujita et al. 2007; Vandenburgh et al. 2008; Johnson et al. 1994; Sathaye et al. 2006).

We found that some of the myotubes start to contract after applying the current pulses for 30–60 min (Supplementary Movie 2), similar to the previous report (Fujita et al. 2007). However, the magnitude of contraction was smaller than expected, probably because the rigidity of the substrate on which the myotubes attached might restrict the contractile degrees of freedom. In order to prepare highly contractile myotubes, we are now planning to reduce the stiffness of the substrate surface.

4 Conclusion

We demonstrated the localized electrical stimulation of C2C12 myotubes using a porous membrane-based culture device that has the several unique technical features. The holes of the PDMS film attached underneath the cell-cultured membrane can condense the electric current induced by a pair of the ring electrodes placed at either side of the membrane. Also, sealing the hole with a bubble prevents the current from passing through the hole. When the current pulses were applied to myotubes differentiated from C2C12 cells cultured on the membrane, externally induced Ca^{2+} transients were reproducibly observed for the cells above the opened hole. We also observed myotube contraction by application of the current pulse for 30–60 min, although the displacement in contraction was not large. We are now attempting to modify the substrate surface for facilitating cellular contraction.

Acknowledgement This study was supported by the Industrial Technology Research Grant Program from NEDO of Japan and by Grants-in-Aid for Scientific Research B (No. 20310070) from the Ministry of Education, Science, and Culture, Japan.

References

H.M. Blau, C.-P. Chiu, C. Webster, Cell **32**(4), 1171–1180 (1983). doi:10.1016/0092-8674(83)90300-8

S.T. Cooper, A.L. Maxwell, E. Kizana, M. Ghoddusi, E.C. Hardeman, I.E. Alexander, D.G. Allen, K.N. North, Cell Motil. Cytoskelet. **58**(3), 200–211 (2004). doi:10.1002/cm.20010

M.B. Davidson, C. Bouch, N. Venkatesan, R.G. Karjala, Am. J. Physiol. Endocrinol. Metab. **267**(6), E808–E813 (1994)

P.G. De Deyne, Am. J. Physiol. Cell Physiol. **279**(6), C1801–C1811 (2000)

R.A. DeFronzo, E. Jacot, E. Jequier, E. Maeder, J. Wahren, J.P. Felber, Diabetes **30**(12), 1000–1007 (1981)

A.J. Engler, M.A. Griffin, S. Sen, C.G. Bonnemann, H.L. Sweeney, D.E. Discher, J. Cell Biol. **166**(6), 877–887 (2004). doi:10.1083/jcb.200405004

H. Fujita, T. Nedachi, M. Kanzaki, Exp. Cell Res. **313**(9), 1853–1865 (2007). doi:10.1016/j.yexcr.2007.03.002

A. Galione, G.C. Churchill, Cell Calcium **32**(5–6), 343–354 (2002). doi:10.1016/S0143416002001902

S.R. Hager, D. Pastorek, A.L. Jochen, D. Meier, Biochem. Biophys. Res. Commun. **181**(1), 240–245 (1991). doi:10.1016/S0006-291X(05)81408-1

T. Hayashi, M.F. Hirshman, E.J. Kurth, W.W. Winder, L.J. Goodyear, Diabetes **47**(8), 1369–1373 (1998). doi:10.2337/diabetes.47.8.1369

T. Ishibashi, K. Takoh, H. Kaji, T. Abe, M. Nishizawa, Sens. Actuators B Chem. **128**(1), 5–11 (2007). doi:10.1016/j.snb.2007.05.027

T.B. Johnson, R.L. Kent, B.A. Bubolz, P.J. McDermott, Circ. Res. **74**(3), 448–459 (1994)

E. Karnieli, M. Armoni, P. Cohen, Y. Kanter, R. Rafaeloff, Diabetes **36**(8), 925–931 (1987). doi:10.2337/diabetes.36.8.925

T. Kislinger, A.O. Gramolini, Y. Pan, K. Rahman, D.H. MacLennan, A. Emili, Mol. Cell. Proteomics **4**(7), 887–901 (2005). doi:10.1074/mcp.M400182-MCP200

A. Klip, T. Ramlal, P.J. Bilan, G.D. Cartee, E.A. Gulve, J.O. Holloszy, Biochem. Biophys. Res. Commun. **172**(2), 728–736 (1990). doi:10.1016/0006-291X(90)90735-6

H.A. Koistinen, J.R. Zierath, Ann. Med. **34**(6), 410–418 (2002). doi:10.1080/07853890232101235l

E.J. Kurth-Kraczek, M.F. Hirshman, L.J. Goodyear, W.W. Winder, Diabetes **48**(8), 1667–1671 (1999). doi:10.2337/diabetes.48.8.1667

P. Lorenzon, A. Bernareggi, V. Degasperi, E. Nurowska, A. Wernig, F. Ruzzier, Exp. Cell Res. **278**(1), 84–91 (2002). doi:10.1006/excr.2002.5562

J.C. Mohr, J.J. de Pablo, S.P. Palecek, Biomaterials **27**(36), 6032–6042 (2006). doi:10.1016/j.biomaterials.2006.07.012

P. Molnar, W.S. Wang, A. Natarajan, J.W. Rumsey, J.J. Hickman, Biotechnol. Prog. **23**(1), 265–268 (2007). doi:10.1021/bp060302q

J.L. Moran, Y. Li, A.A. Hill, W.M. Mounts, C.P. Miller, Physiol. Genomics **10**(2), 103–111 (2002)

J. Mu, J.T. Brozinick, O. Valladares, M. Bucan, M.J. Birnbaum, Mol. Cell **7**(5), 1085–1094 (2001). doi:10.1016/S1097-2765(01)00251-9

T. Nedachi, M. Kanzaki, Am. J. Physiol. Endocrinol. Metab. **291**(4), E817–E828 (2006). doi:10.1152/ajpendo.00194.2006

R. Nesher, I.E. Karl, D.M. Kipnis, Am. J. Physiol. Cell Physiol. **249**(3), C226–C232 (1985)

P. Nuutila, M.J. Knuuti, M. Raitakari, U. Ruotsalainen, M. Teras, L.M. Voipio-Pulkki, M. Haaparanta, O. Solin, U. Wegelius, H. Yki-Jarvinen, Am. J. Physiol. Endocrinol. Metab. **267**(6), E941–E946 (1994)

A. Sathaye, N. Bursac, S. Sheehy, L. Tung, J. Mol. Cell. Cardiol. **41**(4), 633–641 (2006). doi:10.1016/j.yjmcc.2006.06.076

K. Takoh, A. Takahashi, T. Matsue, M. Nishizawa, Anal. Chim. Acta **522**(1), 45–49 (2004). doi:10.1016/j.aca.2004.06.053
K. Takoh, T. Ishibashi, T. Matsue, M. Nishizawa, Sens. Actuators B Chem. **108**(1–2), 683–687 (2005). doi:10.1016/j.snb.2004.12.090
L.L. Tortorella, P.F. Pilch, Am. J. Physiol. Endocrinol. Metab. **283**(3), E514–E524 (2002)
A. Tourovskaia, T.F. Kosar, A. Folch, Biophys. J. **90**(6), 2192–2198 (2006). doi:10.1529/biophysj.105.074864
H. Vandenburgh, J. Shansky, F. Benesch-Lee, V. Barbata, J. Reid, L. Thorrez, R. Valentini, G. Crawford, Muscle Nerve **37**(4), 438–447 (2008). doi:10.1002/mus.20931
H. Wallberg-Henriksson, N. Zetan, J. Henriksson, J. Biol. Chem. **262** (16), 7665–7671 (1987)
T. Walles, M. Weimer, K. Linke, J. Michaelis, H. Mertsching, Onkologie **30**(7), 388–394 (2007). doi:10.1159/000102544
K. Wilson, P. Molnar, J. Hickman, Lab Chip **7**(7), 920–922 (2007). doi:10.1039/b617939h
D.C. Wright, K.A. Hucker, J.O. Holloszy, D.H. Han, Diabetes **53** (2), 330–335 (2004). doi:10.2337/diabetes.53.2.330
D. Yaffe, O.R.A. Saxel, Nature **270**(5639), 725–727 (1977). doi:10.1038/270725a0

Journal of Biomechanical Science and Engineering

Vol. 3, No. 4, 2008

Characterization of Motility Properties of Kinesin-Driven Microtubules Towards Nano-Scale Transporter: Focusing on Length of Microtubules and Kinesin Density*

Shukei SUGITA**, Naoya SAKAMOTO***, Toshiro OHASHI*** and Masaaki SATO**,***

**Department of Biomedical Engineering, Graduate School of Biomedical Engineering, Tohoku University,
6-6-01 Aoba-yama, Sendai 980-8579, Japan
E-mail: s_sugita@bml.mech.tohoku.ac.jp

***Department of Bioengineering and Robotics, Graduate School of Engineering, Tohoku University,
6-6-01 Aoba-yama, Sendai 980-8579, Japan

Abstract

Kinesins, biomolecular motors moving along microtubules (MTs) in cells, can potentially be utilized as nano-scale transport systems with an inverted gliding assay, in which the MTs glide on a kinesin-coated surface. Although the key requirements include controls of gliding direction and velocity of MTs, the details of motility properties of MTs have not been well known. In this study, we quantitatively measured angular and gliding velocities, particularly focusing on the effects of MT length and kinesin density. The gliding assay of MTs of up to 20 μm in length was performed on a substrate coated with the kinesin density of 7.5, 38, and 75 μg/ml that resulted in the kinesin spacing of 7.8, 4.2, and 3.1 μm, respectively. The angular velocity for MTs shorter than kinesin spacings significantly decreased with increasing their length, and that for MTs longer than kinesin spacings was not affected by their length. Moreover, the angular velocity was substantially higher at lower kinesin density. These results suggest that both the number of associated kinesins with MTs and the kinesin spacings may contribute to the gliding direction. In contrast, the gliding velocity was independent of the MT length, ranging from 0.3 to 0.5 μm/s with decreasing the kinesin density. This may potentially imply the existence of an underlying mechanism with respect to the number of kinesins per the unit length of MTs. Towards development of high throughput nano-scale transport systems, long MTs and low kinesin densities would be effective for high directionality and high velocity, respectively.

Key words: Nanoscale Transport System, Motor Protein, Microtubule, Angular Velocity, Gliding Velocity

1. Introduction

Kinesin-1 (formerly conventional kinesin) is one of motor proteins that move unidirectionally along microtubules (MTs) in cells. Kinesins are constituted of the motor domains at the N-terminal, coiled-coil regions, and tail regions, with approximately 60 nm in contour length [1] and transport cargos such as vesicles and organelles using energy derived from ATP hydrolysis [2, 3]. Recently, many attempts utilizing kinesin motor proteins have been made for developing nano-scale transport systems *in vitro* [4, 5] because the biological nanomachines have several advantages compared to artificial actuators. Firstly,

*Received 9 June, 2008 (No. 08-0406)
[DOI: 10.1299/jbse.3.510]